Chemosphere 376 (2025) 144262

Contents lists available at ScienceDirect

Chemosphere

journal homepage: www.elsevier.com/locate/chemosphere

# Mercury dynamics in the mangrove-influenced estuary of the Parnaíba Delta, Brazil

Andreia C.M. Rodrigues [a,*], Natalia Torres-Rodriguez [a], Jingjing Yuan [a,b], Aurélie Dufour [a], Luiz Drude de Lacerda [c], Lars-Eric Heimbürger-Boavida [a]

[a] Aix Marseille Université, CNRS/INSU, Université de Toulon, IRD, Mediterranean Institute of Oceanography (MIO), Marseille, France
[b] Institute of Surface-Earth System Science, School of Earth System Science, Tianjin University, Tianjin, 300072, China
[c] Laboratório de Biogeoquímica Costeira, Instituto de Ciências do Mar, Universidade Federal do Ceará, Av. Abolição 3207, Fortaleza, 60.165-081, CE, Brazil

## HIGHLIGHTS

- This study gives critical baseline data on mercury dynamics in a pristine mangrove system.
- Low tHg and dMeHg levels confirm the pristine state of the Parnaíba River Delta.
- Tidal exchange with the ocean is associated to low Hg levels.
- Particulate Hg is effectively sequestered to fine-grained mangrove sediments.
- Pristine mangroves act as a blue carbon and blue mercury ecosystem.

## GRAPHICAL ABSTRACT

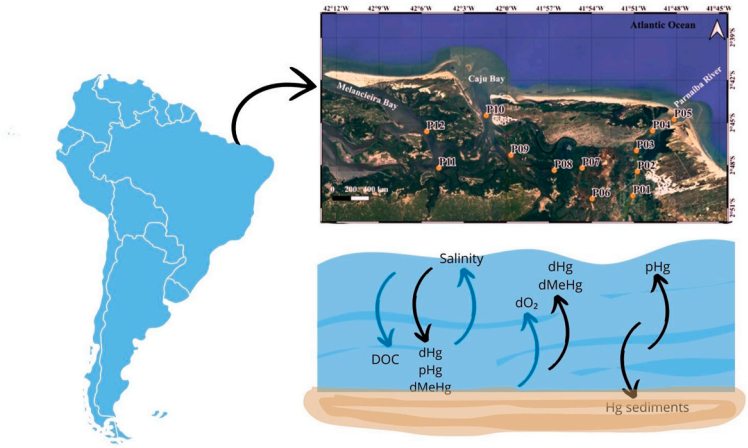


## ARTICLE INFO

Handling Editor: Milena Horvat

*Keywords:*
Hydrochemistry
Estuary
Mercury speciation
Mangrove
Blue carbon
Blue mercury

## ABSTRACT

The Parnaíba River Delta (PRD), located in northeastern Brazil, is an ecologically crucial estuarine system little impacted by anthropogenic activities. This study aimed to assess mercury (Hg) contamination levels in the water and sediments and their link to changes in the hydrographic parameters across the delta to evaluate spatial distribution patterns and Hg speciation. Water and surface sediment samples were collected from 12 stations throughout the PRD. Results showed that total Hg (tHg) levels ranged from 4.27 to 39.01 pM, with the majority associated with particles (pHg: 16.03 ± 9.95 pM). Dissolved methylmercury concentrations (dMeHg: 0.043 ± 0.015 pM) were low and represented a minor fraction of Hg. Seawater intrusion during flood tide was associated with lower levels of all Hg species. Particulate Hg was sequestered and stored in the fine-grained mangrove sediments (0.14–28.2 ng $g^{-1}$ dry weight). Our study provides baseline data on Hg cycling in the PRD,

* Corresponding author.
*E-mail addresses:* andreia.rodrigues@mio.osupytheas.fr (A.C.M. Rodrigues), natalia.torres-rodrigues@mio.osupytheas.fr (N. Torres-Rodriguez), jingjingyuan.2021@gmail.com (J. Yuan), aurelie.dufour@mio.osupytheas.fr (A. Dufour), ldrude1956@ufc.br (L. Drude de Lacerda), lars-eric.heimburger@mio.osupytheas.fr (L.-E. Heimbürger-Boavida).

https://doi.org/10.1016/j.chemosphere.2025.144262
Received 30 November 2024; Received in revised form 20 February 2025; Accepted 25 February 2025
Available online 4 March 2025

highlighting its pristine condition and function as a buffer between terrestrial and marine environments. Pristine mangrove systems are effectively sequestering carbon and mercury and should, therefore, be considered as blue carbon and blue mercury ecosystems for mitigation strategies.

## 1. Introduction

Mercury (Hg) contamination is a global environmental issue that threatens human health and ecosystems (Outridge et al., 2018). Mercury is a toxic trace metal that can bioaccumulate in organisms, leading to adverse effects, including neurological damage, reproductive failure, and even death. Recent decades have witnessed extensive investigations into Hg biogeochemistry across terrestrial, atmospheric, and aquatic systems, with a growing focus on coastal ecosystems (Lei et al., 2019; Liu et al., 2021; Sonke et al., 2013). Coastal environments play a pivotal role in the global Hg cycle, functioning not only as repositories for Hg transported from terrestrial sources but also as potential contributors to the ocean (Cossa et al., 2024; Fitzgerald et al., 2007; Liu et al., 2021).

In coastal areas, Hg behaves uniquely compared to other trace metals because of the diverse range of dissolved Hg species in the water (Horvat, 1997) and the potential evasion of gaseous Hg species (Fisher et al., 2012). Dissolved Hg species in estuarine waters exhibit complex behavior due to the mixing of freshwater and seawater, as well as the presence of suspended particulate matter (SPM) and dissolved organic matter (DOM) (Coquery et al., 1995). The dominant dissolved Hg species include inorganic divalent mercury ($Hg^{2+}$), methylmercury (MeHg), and elemental mercury ($Hg^0$) (Ullrich et al., 2001a). $Hg^{2+}$ tends to form strong complexes with DOM and chloride ions, with the relative importance of these complexes varying along the salinity gradient. MeHg, the most toxic and bioaccumulative Hg species, exists primarily in two forms: monomethylmercury (MMHg) and dimethylmercury (DMHg). MeHg is produced by anaerobic bacteria through the methylation of inorganic Hg species, and its distribution is influenced by factors such as redox conditions, organic matter content, and sulfide concentrations (Cabrol et al., 2023; Rosati et al., 2018; Villar et al., 2020). Dissolved gaseous $Hg^0$ is produced through biotic and abiotic reduction processes, and its concentration is controlled by the balance between reduction and oxidation reactions, as well as air-water exchange. The partitioning and speciation of dissolved Hg species in estuaries are further complicated by the formation of colloidal complexes, adsorption onto suspended particles, and flocculation processes (Gworek et al., 2016). Particulate mercury (pHg) plays a significant role in areas characterized by high primary productivity and coastal regions (Cossa et al., 2018; Fitzgerald et al., 2007). The divalent form of Hg ($Hg^{2+}$) exhibits an especially strong affinity for particles in the water column (Lamborg et al., 2016; Tesán-Onrubia et al., 2020). This diversity, along with Hg high reactivity, leads to important speciation changes in estuarine environments, potentially affecting its bioavailability along estuarine gradients (Lacerda et al., 2001a). Mangroves are particularly important for the marine biochemical cycle of dissolved organic carbon (DOC), contributing up to 15% to coastal sediment carbon storage and approximately 10% to the export of particulate terrestrial carbon to the ocean (Lei et al., 2019).

Recent research has advanced our understanding of rivers (Liu et al., 2021), submarine groundwater discharge (Aleku et al., 2024), and atmospheric inputs (Jiskra et al., 2021) to the ocean. Mercury cycling in mangrove estuaries remains understudied. These results notwithstanding, research on Hg levels and biogeochemical mercury cycling in mangrove areas is still limited compared to other metals (Lacerda et al., 2022), and the importance of continuous monitoring and studying the direct impact of the site-specific contamination on the local food web and the ecosystem has been highlighted (Lei et al., 2019; Viana et al., 2023). Mercury methylation in mangrove sediments and the subsequent release of MeHg into adjacent waters might influence the local and global Hg cycling dynamics. Bergamaschi et al. (2012) estimated that mesohaline estuarine mangrove swamps of the Shark River estuary (Everglades National Park, Florida, USA) reinforced the tidal-driven contribution of these systems with 10% of the global terrestrial flux of DOC, and estimated yields of Hg (tHg: 28 ± 4.5 μg $m^{-2}$ $yr^{-1}$; MeHg: 3.1 ± 0.4 μg $m^{-2}$ $yr^{-1}$) to nearby coastal waters. A study in the La Puntilla estuary in Ecuador has shed light on the presence of Hg in mangrove sediments and has highlighted its potential ecological and human health risks (Velásquez-López et al., 2020).

Mangrove ecosystems epitomize evergreen ecosystems persistently distributed along the gradient from mean sea level to the zenith of the highest spring tide across tropical and subtropical regions. Flourishing under stressful environmental conditions, encompassing substantial tidal amplitude differentials, high salinity, elevated thermal regimes, and anoxic, silt-laden substrates, these ecosystems assume a paramount role in buttressing human socio-environmental equilibrium (Awuku-Sowah et al., 2022). Ecosystem services provided by mangrove systems play a vital role in human sustainability, including nutrient cycling, soil formation, wood and food production. They also hold great ecological relevance, serving as nurseries and habitat for several marine species, and carbon reservoirs, being one of the most productive and biologically complex ecosystems on earth (Rovai et al., 2022). Brazil boasts the second-largest mangrove area globally (Diniz et al., 2019; Rovai et al., 2022). Mangrove areas are important for stabilizing coastal areas and reducing erosion, with the benefits provided by these systems of flood protection estimated to be around $US 65 billion per year (Menéndez et al., 2020). Moreover, mangrove's complex root systems increase particle deposition from the water, improving the water quality flowing from rivers and streams into the estuarine and ocean systems (Awuku-Sowah et al., 2022). The high productivity, abundant organic matter, and complex root systems of mangroves create ideal conditions for trapping and retaining particulate matter, including Hg-bound particles from both terrestrial and aquatic sources, making them key areas for the transport, transformation, and accumulation of particulate Hg. In sediments, most chalcophile metals, including Hg, predominantly accumulate as species that exhibit low bioavailability. This, together with the typical high sediment accretion rates, play a vital role in mitigating metal contamination (Lacerda et al., 2022). However, there is currently no consensus regarding whether mangrove ecosystems act primarily as sources or sinks for Hg and MeHg. Some studies have shown that mangroves can efficiently sequester and retain Hg in their sediments over decades, suggesting they function as long-term sinks (Castro et al., 2021). However, other research indicates that mangroves may also serve as sources of Hg and MeHg to adjacent coastal waters, particularly during periods of tidal flushing or heavy rainfall (You et al., 2024). Huang et al. (2020) highlighted the importance of seawater inputs and tidal action on Hg biogeochemical cycling on mangrove systems, with sediments from two mangroves from China serving as sinks for Hg after atmospheric deposition into seawater and functioning as a source of up to 40 % of Hg to the coastal ocean. Contrastingly, an assessment of several metals but not Hg in the sediments of the Parnaíba River Delta (PRD), located in the semi-arid coast of northeastern Brazil, described this area as having a pristine condition, except for the more urbanized Igaraçú channel near Parnaíba city (Paula Filho et al., 2021). Mangroves can act as a Hg sink when deposited under anoxic conditions and immobilized as sulfides or coprecipitated with pyrites (Lacerda et al., 2022). On the other hand, mangroves can be a source of Hg when the precipitated compounds are oxidized by radial oxygen loss due to oxygen diffusion from mangrove roots or erosion or deforestation, releasing Hg to porewaters, where it can complex and be exported with DOC (Lacerda et al., 2020). Despite their potential importance in Hg

cycling, mangrove ecosystems are not yet considered in global budgets and models. This omission represents a significant gap in our understanding of Hg dynamics in coastal environments, particularly as mangroves are widespread in tropical and subtropical regions where Hg contamination can be a concern.

In the face of escalating environmental and health apprehensions associated with Hg contamination and robust information about Hg in the environment to fulfil Minamata Convention goals, the intricate mechanisms governing the dynamics of Hg within mangrove ecosystems have received limited investigative attention. This conspicuous paucity of research underscores the need for a more concerted scientific endeavor to comprehend the complex behavior of Hg in mangroves, which is paramount considering the mounting ecological and human health implications.

Furthermore, this semi-arid coastal region is experiencing great impacts due to climate change, including altered hydrodynamics and increasing marine influence. These changes have led to reduced continental runoff into the ocean due to decreased rainfall and damming of rivers. Along with heat accumulation in the South Atlantic, a positive feedback loop is created, resulting in prolonged water residence time in estuaries, extending saline intrusion, sediment accumulation, and the expansion of mangroves. Mercury dynamics show that higher concentrations and fluxes occur from rivers to estuaries, accumulating as particulate Hg within estuaries. Dissolved and reactive Hg fluvial fluxes are minimal during rainy periods but increase during the dry season. Conversely, while deposition to mangrove sediments reduces Hg bioavailability (Lacerda et al., 2020), the export of dissolved Hg species from mangroves, mainly during the dry season, might increase Hg bioavailability. Overall, changing coastal sedimentation-erosion equilibrium or climate dynamics, may increase Hg accretion to and fixation in mangrove sediments. If, for example, the sediment load of rivers is increased by basin land use, such as agriculture, or if conditions become drier, like in NE Brazil, where the dry season is extended, this amplifies the export of dissolved Hg and increases the risk of contamination in estuarine and coastal ecosystems. Changes in hydrodynamics also affect the production and degradation of MeHg in mangrove sediments by influencing redox conditions, microbial activities, and the availability of dissolved reactive Hg, all variables that significantly impact rates of Hg methylation and demethylation (Cossa et al., 2014; Eom et al., 2024; Liem-Nguyen et al., 2016). Therefore, it is highly probable that a similar pattern observed for total dissolved Hg occurs for MeHg, with mangroves also exporting this toxic Hg species, mostly during dry periods. Unfortunately, however, the very limited data on MeHg concentrations, cycling, and fluxes in mangrove ecosystems may impair generalizations (Lei et al., 2019).

Thus, our study aims to investigate the distribution of Hg and its partitioning along the mangrove system of the PRD, as this is a unique pristine delta, which is not directly affected by anthropogenic activities. We collected water and sediment samples from 12 stations within the study area. Specifically, we examined these Hg species in the dry season and throughout a tidal cycle. Extended water residence times during dry periods are anticipated to prolong exposure to higher salinity in the upper estuary, potentially enhancing the mobilization of Hg, favoring its complexation with available organic matter, and facilitating Hg transport downstream to lower estuarine regions, where it bioaccumulates. This increase in complexation is likely due to incomplete organic matter degradation by anaerobic microorganisms under prolonged flooded conditions with low freshwater input, as reported in other NE Bazil estuaries (Lacerda et al., 2020; Soares et al., 2021). The findings of our study provide new and valuable information for the ecological risk assessment and management of Hg contamination in mangrove systems.

## 2. Material and methods

### 2.1. The Parnaíba River Delta

The study was conducted in the PRD, located in the Equatorial Zone of Northeast Brazil, between the states of Piauí and Maranhão. The PRD system is a complex and ecologically relevant ecosystem, providing habitats for diverse plant and animal communities. The total area of the delta is about 2700 $km^2$ and is encircled by an Environmental Protection Area (EPA), a 3138 $km^2$ federal conservation unit established in 1996 and located at 02°37′– 03°05′ S and 42°29′– 41°09′ W (Fig. 1). Within the Delta, there are over 1500 $km^2$ of pristine mangroves and associated ecosystems. The dominant tree species are *Rhizophora mangle*, *Avicennia germinans* and *Laguncularia racemosa*. Trees are tall, reaching over 20 m, and since the region is located in a transition climate zone, many typical Amazon species from flooded forests, such as the aquatic macrophytes *Montrichardia linifera* and *Eichhornia azurea*, and palms (mostly Arecaceae) abound, mixed with mangroves at the higher estuary. Along the eastern sector, actively migrating coastal dunes frequently advance over mangroves, whereas in the western portion, tidal channels occur between mangrove islands and deltaic plains (Szczygielski et al., 2015).

This climatic transition zone between the Semi-Arid and Pre-Amazon typically presents two marked seasons: a dry period when semi-arid conditions dominate, from July–August to December, and a wet season from January to May–June, when higher rainfall results in large riverine contribution (Andrade et al., 2005). The Parnaíba River, the third largest in Brazil with a length of 1400 km and over 34,000 $km^2$ of basin area, contributes a substantial freshwater flow ranging from 240 to nearly 3000 $m^3\ s^{-1}$ (average 600 $m^3\ s^{-1}$) (INMET, 2023; Paula Filho et al., 2015; SNIRH, 2023). The river's discharge into the PRD divides into 5 major canals that flow through 73 islands, mostly colonized by mangroves, that are partially flooded during high tides. During the ebb period, mangrove creeks in these islands significantly contribute to surface and porewaters, since changing hydrostatic pressure gradients between flood and ebb periods trigger porewater exchange between mangrove soils and surface waters. Although no data on mangrove porewater contribution to the main canals of the PRD exists, pore water tidal pumping in mesotidal mangroves, recently reviewed by Cabral et al. (2024), suggests a contribution ranging from 12 ± 10% of the total flow. At a fixed station (P8, see sampling design below), temporal variability of ADCP-obtained water flows ranged from 240 to 616 $m^3s^{-1}$, average 432 $m^3s^{-1}$, during the ebb period and from −130 to −334 $m^3s^{-1}$, average −263 $m^3s^{-1}$, during the flood period. Therefore, flows show a greater competence in ebb tide conditions, even with the campaign being carried out in the dry season (Santos and Lima, 2022).

The region is influenced by the Intertropical Convergence Zone (ITCZ) and the South Atlantic anticyclone. Annual rainfall averages 1152 mm (Chielle et al., 2023). The duration of each season is influenced by the position of the ITCZ and the occurrence and intensity of the El Niño-Southern Oscillation (Hastenrath, 2006). The PRD is a mesotidal estuary with a semidiurnal tide regime with a maximum height of 3.3 m during spring tide and 1.7 m during neap tide. Northeast winds prevail throughout the year, with average speeds ranging from 2 to 6 m $s^{-1}$ (Bittencourt et al., 2005).

### 2.2. Sampling design and collection

The sampling campaign was conducted at various locations within the PRD under the spring tide regime during the end of the dry season of 2021 (Fig. 1). Water and sediment samples (12 stations and one anchoring at station 8, Fig. 1) were collected using a trace metal clean 5 L GOFLO (General Oceanics) and a custom-made push corer, respectively. We sampled a sediment core to obtain porewaters at the P7 station, at the border of the mangrove. The sampling locations were strategically selected to cover a range of environmental conditions and potential anthropogenic contributions. Surface water temperature,

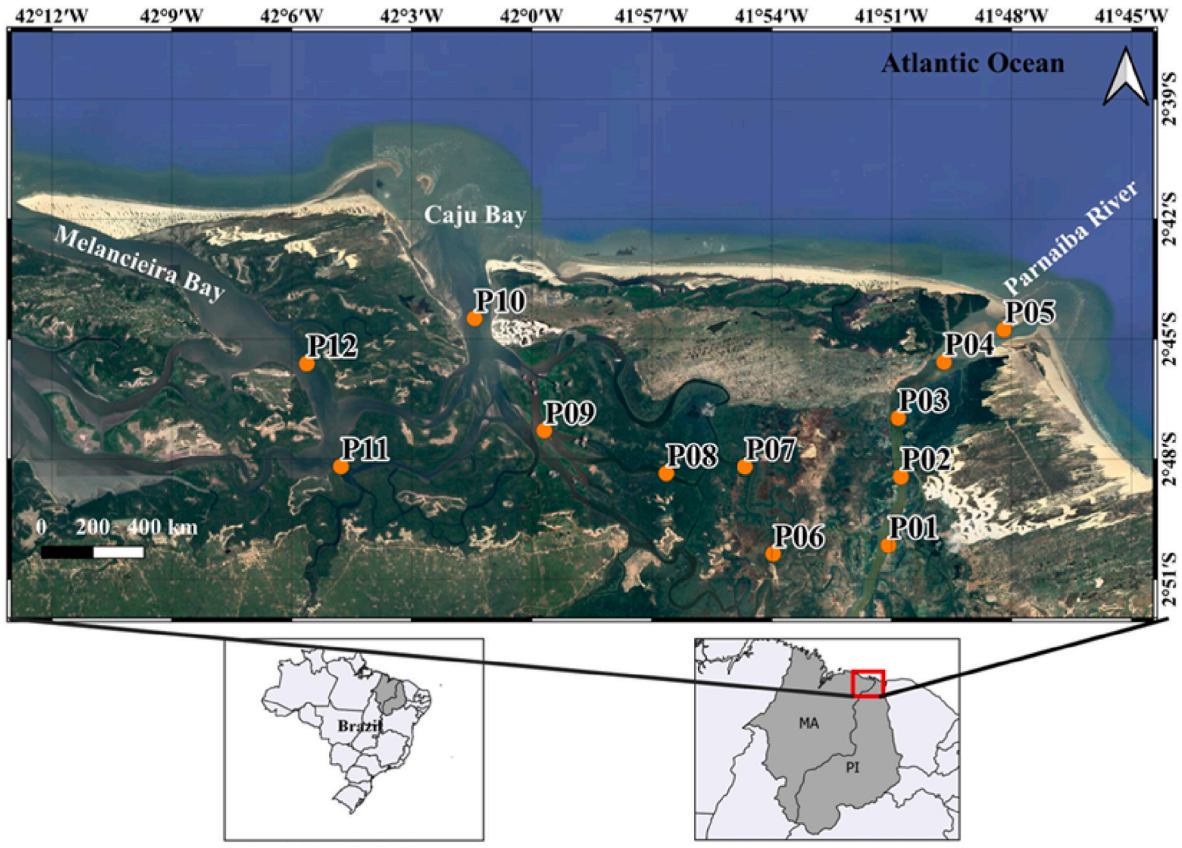


**Fig. 1.** Map showing the Paraíba River Delta (PRD) in the transition zone between the semi-arid and humid climate in NE Brazil. Hydrographic stations and sampling sites (P1 – P12), fixed tidal station (P8).

conductivity, pH, and dissolved oxygen (DO) were measured using a Conductive-Temperature-Depth - CTD (EXO2/YSI). DOC was analyzed by acidifying and purging a 4.0 mL aliquot with $CO_2$-free nitrogen, followed by high-temperature catalytic oxidation using a TOC 5000 Shimadzu analyzer, with phthalate solution as the standard (Lacerda et al., 2001b).

### 2.3. Sampling and mercury analysis

Filtration for dHg, dMeHg, and pHg was realized by pressurizing the GOFLO bottle to 0.5 bar with nitrogen gas at the top valve and using pre-combusted glass fibre filters (GF/F, 0.7 μm, Millipore) loaded in acid-cleaned perfluoroalkoxy (PFA) Savillex filter holders at the bottom valve (Suppl. Mat. Fig. S1). This setup, inspired by the GEOTRACES cookbook (GEOTRACES, 2017), avoids possible contamination and can be done in the field where no clean container or laminar flow hood are available. Filtered water MeHg samples were acidified to 0.5 % v:v with double distilled hydrochloric acid (HCl). Filtered dHg samples were not acidified in the field to avoid potential contamination. The GF/F filter was retrieved after filtering 0.5–3.75 L for pHg analysis. Sediment grab samples were taken by hand, and we sampled porewater run off during low tide directly into 60 mL glass vials (tHg) and 125 mL PET bottles for MeHg. Sediments and GF/F filters were stored in double-bag plastic bags and kept refrigerated for transport.

The tHg and dHg were measured by cold vapor atomic fluorescence (CV-AFS) (Heimbürger et al., 2015) according to US Environmental Protection Agency (US EPA) Method 1631. Powders of potassium bromide (KBr) and potassium bromate $KBrO_3$ (Sigma Aldrich) were heated for 4 h at 250 °C to ensure cleanliness. The Hg-free powders were used together with bidistilled HCl to prepare a solution of bromine monochloride (BrCl). For the analyses, BrCl was added in excess, equivalent to 0.1–0.5 % of the sample volume. The sample was left to react for 20 min or until the yellow color persisted. After oxidation, 20–35 mL of the sample was added to a FEP Teflon impinger and reduced with stannous chloride ($SnCl_2$). The resultant $Hg^0$ was transported with argon gas to a custom-made purge and trap system, amalgamated onto a gold trap, thermally decomposed, and analyzed by an atomic fluorescence spectrometer (Brooks and Rand, Model 3). The measurements were calibrated with a 7-point calibration curve ($R^2 > 0.9998$) constructed with reference material NIST-3133. The certified reference materials ORMS-5 (certified range 131 ± 6.5 pM, National Research Council Canada) and ERM-CA400 (certified range 83.8 ± 5.5 pM, European reference materials) were analyzed at the beginning and end of each session for quality control. The CRMs were always within the certified range. Standard bracketing with reference material NIST-3133 was carried out every 2 to 6 samples to account for the drift of the machine.

The dMeHg concentrations in the water samples were measured using a Gas Chromatography Sector Field Inductively Coupled Plasma Mass Spectrometry (GC–SF–ICP-MS) and quantified via isotopic dilution (Heimbürger et al., 2015; Monperrus et al., 2005). Glass bottles of 140 mL capacity were heated to 450 °C for 4 h to remove Hg traces. Approximately 110 mL of the sample was added to the bottles, together with 1 mL of sodium acetate buffer solution (ULTREX II Ultrapure Reagent, J.T. Baker). After buffer equilibration, the pH was adjusted to 4.2 using 100–400 μL ammonia ($NH_3$) (ULTREX II Ultrapure Reagent, J.T. Baker). Subsequently, isotopically enriched spikes were added in excess (4.2 for $i^{199}Hg$ and 5.1 for $MM^{201}Hg$, ICS, Spain). A 5% v/v tetrapropylborate solution (Merseburger Spezialchemikalien) and 150 μL of isooctane (Sigma Aldrich) were added after pH adjustment. The bottles were then sealed with Teflon-lined crimp caps (Fisherbrand) and shaken for 15 min on an orbital shaker (Edmund Buhler KS15). After shaking, the organic phase containing the derivatized Hg species was transferred to vials for injection into a GC (THERMO GC 1300 with GC220 transfer module) coupled to a SF-ICP-MS (Thermo Element XR). The detection

limit was 0.001 pM at a signal-to-noise ratio of 3:1. To confirm the spike concentration (96.6 ± 7.9%), reverse isotopic dilution was conducted using a MeHgCl standard (Brooks Rand) traceable to NIST1641E.

Prior to pHg analysis, the filters were freeze-dried (Christ Gamma 1–16 LSCplus) for 48 h. The Hg concentrations in the freeze-dried filter (pHg) and homogenized sediment samples (Hg sed) were measured by a cold vapor atomic absorption spectrometry (AAS, LECO AMA 254) according to the US Environmental Protection Agency (US EPA) method 7473. Between 120 and 150 mg of each sediment sample and filter was placed in a cleaned nickel vessel and thermally decomposed in an oxygen gas stream. Then the Hg was selectively trapped with gold amalgamation, heated, desorbed, and detected by AAS with a low-level optical cell. Calibration was performed using a NIST-3133 certified standard solution that was checked daily against the certified reference material marine sediment MESS-4 (National Research Council of Canada; 90 ± 40 ng $g^{-1}$), and always found within the certified range.

### 2.4. Data analysis

Multivariate data analyses were performed using principal component analysis (PCA) after data standardization. PCA is a widely used exploratory data analysis tool that identifies patterns and relationships between variables and observations. By plotting the loadings of these data's principal components (PC1 and PC2), we can identify groups of samples with similar behaviour and the existing association among the original variables. The Pearson correlation analysis was applied to confirm the relationship between variables in evaluating Hg changes with water parameters and during a tidal cycle. This analysis helped assess the strength and direction of the relationships between variables. All statistical analyses were set at a significance level of 5 % and

**Table 1**
Values for water parameters (salinity, temperature – T, pH, dissolved oxygen – DO, dissolved organic carbon – DOC) and mercury species (particulate mercury – pHg, dissolved mercury – dHg, dissolved methylmercury – dMeHg) measured in waters and sediments (Hg sed) of the PRD at the studied hydrological stations. - stands for not analyzed.

| Station | Date | Time (h) | Salinity | T (°C) | pH | DO (μM) | DOC (μM) | pHg (pM) | dHg (pM) | dMeHg (pM) | Hg sed (ng $g^{-1}$) |
|---|---|---|---|---|---|---|---|---|---|---|---|
| P1 | 07/12/21 | 12:03 | 0.10 | 29.0 | 8.60 | 199 | 2.66 | 14.73 | 3.13 | – | 0.17 |
| P3 | 07/12/21 | 10:44 | 0.30 | 29.7 | 8.67 | 178 | 2.45 | 11.27 | 2.0 | 0.045 | 0.24 |
| P4 | 07/12/21 | 9:30 | 0.30 | 29.4 | 7.23 | 222 | 3.15 | 21.18 | 2.33 | 0.060 | – |
| P5 | 07/12/21 | 9:00 | 13.7 | 29.2 | 6.48 | 165 | 2.76 | 7.70 | 1.16 | 0.053 | 0.20 |
| P6 | 07/12/21 | 13:55 | 0.10 | 30.7 | 9.13 | 229 | 2.86 | 10.62 | 3.11 | 0.073 | 0.16 |
| P7 | 07/12/21 | 15:30 | 0.32 | 31.6 | 6.80 | 224 | 4.53 | 24.97 | – | 0.054 | – |
| P8 | 07/12/21 | 20:30 | 30.5 | 29.1 | 7.35 | 72 | 2.12 | – | – | – | – |
| | 07/12/21 | 21:30 | 30.2 | 29.6 | 8.12 | 220 | 1.43 | – | – | – | – |
| | 07/12/21 | 22:39 | 28.6 | 29.2 | 8.20 | 156 | 1.45 | 10.27 | 0.34 | 0.041 | – |
| | 07/12/21 | 23:30 | 26.4 | 29.8 | 7.83 | 201 | 1.88 | – | – | – | – |
| | 08/12/21 | 0:30 | 19.7 | 28.5 | 7.95 | 236 | 2.59 | 13.42 | 1.23 | 0.037 | 0.15 |
| | 08/12/21 | 1:30 | 13.9 | 28.9 | 5.85 | 96 | 7.34 | – | – | – | – |
| | 08/12/21 | 2:30 | 10.5 | 29.7 | 7.77 | 124 | 3.47 | 35.23 | 1.67 | 0.036 | – |
| | 08/12/21 | 3:30 | 9.07 | 30.6 | 7.18 | 188 | 3.54 | – | – | – | – |
| | 08/12/21 | 4:30 | 10.0 | 26.3 | 7.54 | 248 | 3.57 | 36.98 | 2.03 | – | – |
| | 08/12/21 | 5:30 | 14.8 | 30.2 | 7.25 | 187 | 3.25 | – | – | – | – |
| | 08/12/21 | 6:40 | 20.7 | 29.3 | 7.59 | 182 | 2.91 | 16.79 | 1.07 | 0.031 | – |
| | 08/12/21 | 7:30 | 24.9 | 29.7 | 7.74 | 196 | 2.20 | – | – | – | – |
| | 08/12/21 | 8:40 | 27.3 | 29.3 | 8.02 | 154 | 2.26 | 12.81 | 1.02 | – | – |
| | 08/12/21 | 9:30 | 28.6 | 29.3 | 8.08 | 159 | 1.85 | – | – | – | – |
| P9 | 08/12/21 | 18:20 | 30.0 | 28.9 | 7.50 | 156 | 1.74 | 11.67 | 1.29 | 0.031 | 0.14 |
| P10 | 08/12/21 | 10:45 | 28.2 | 29.6 | 8.09 | 144 | 2.28 | 1.80 | – | 0.026 | 4.90 |
| P11 | 08/12/21 | 12:20 | 30.0 | 29.6 | 8.07 | 147 | 3.21 | 25.63 | – | – | – |
| P12 | 08/12/21 | 14:57 | 29.4 | 30.4 | 8.14 | 168 | 2.60 | 2.63 | 1.64 | 0.025 | – |
| | 08/12/21 | 14:57 | 29.4 | 30.7 | 8.26 | 215 | 2.60 | 14.73 | 3.13 | – | – |
| Mean ± SD | | | 18.3 ± 11.6 | 29.5 ± 1.0 | 7.74 ± 0.71 | 178 ± 43 | 2.83 ± 1.19 | 16.03 ± 9.95 | 1.80 ± 0.87 | 0.043 ± 0.015 | 0.85 ± 1.79 |

performed using the software GraphPad Prism version 9.5.0 (La Jolla, California).

## 3. Results

### 3.1. Water parameters

The salinity distribution exhibited a substantial gradient across all sampled stations, spanning a range of 30.4. The lowest salinity value of 0.10 was observed at P1 and P6, while the highest salinity of 30.50 was recorded at P8 (Suppl. Mat. Fig. S2). Temperature exhibited a spatial range of 5.3 °C. The lowest temperature, 26.3 °C, was registered at P8, whereas the highest temperature, 31.6 °C, was observed at P7. The pH exhibited a range of 3.28, with a minimum of 5.8 (P8) and a maximum of 9.13 (P6). High dissolved oxygen (DO) concentrations were observed, with a range of 176 μM. The minimum DO concentration was 72 μM, while the maximum was 248 μM, both measured at P8 during the tidal cycle assessment. Similarly, DOC concentrations highest values, varying from 1.43 to 7.34 μM, were observed at P8. Table 1 shows values measured in waters of the PRD.

### 3.2. Mercury in the water, sediments and pore water

Table 1 contains the Hg values obtained from various hydrological stations. Higher values of pHg (>20 pM) were measured at stations P4, P7, P8 and P11. For dHg, higher values (≥2 pM) were observed at P1, P3, P4, P6, P8 and P12. With the exception of P12, located on Melancieria bay, all other stations are innermost stations of the Parnaíba river, surrounded by mangroves (Fig. 1) and stronger fluvial influence (Suppl. Mat. Fig. S2). dMeHg accounted for 2 - 5 % of dHg, except at P8 station (22h39, low tide) when dMeHg reached 12 % of dHg (Table 1).

The PCA distinguished two groups of variables based on two principal components (PC) that jointly explained 79.5 % of the total data variance (Fig. 2a). Principal component 1 captured 55.1 % of the variance, primarily represented by the variables DO, dHg and salinity (Table 2, Fig. 2b). The PC2 accounted for 24.4 % of the variance and was mainly represented by temperature, pHg and pH (Table 2, Fig. 2b).

Hg concentrations in the sediments varied from 0.14 (P9) to 4.9 (P10) ng $g^{-1}$ dry weight (dw, Table 1). At P6, extra samplings on the riverside showed higher levels of Hg (21.6 - 22.01 ng $g^{-1}$ dw), similar to P7 surface and deep sediments layers with 26.7 and 28.2 ng $g^{-1}$ dw of Hg, respectively. Porewater analysis showed a tHg concentration of 14.3 pM.

pHg showed a significant positive correlation with DOC and a negative correlation with Hg in sediments (Table 3). Not surprisingly, dHg showed a significant negative correlation with salinity and positive significant correlations with DO and DOC (Table 3). A significant negative correlation was observed between dMeHg and salinity, juxtaposed with significant positive correlations with DO (Table 3).

**Table 2**
Correlation coefficients of each variable to the principal components (PC).

| | PC1 | PC2 |
|---|---|---|
| Salinity | 0.901 | −0.225 |
| T | −0.431 | −0.821 |
| DO | −0.959 | 0.045 |
| pH | −0.414 | −0.632 |
| DOC | −0.807 | 0.075 |
| pHg | −0.504 | 0.755 |
| dHg | −0.930 | −0.076 |

### 3.3. Tidal cycle variability at hydrographic station P8

At hydrological station P8, a detailed examination was conducted to assess the temporal fluctuation of pHg, dHg and dMeHg in response to variations in water parameters throughout one tide cycle (Table 1 and Fig. 3). During the tidal oscillation, salinity presented a significant negative correlation with DOC ($r$ = -0.94, p = 0.005). On the other hand, dHg showed a significant negative correlation with salinity ($r$ = -0.93, p = 0.008) but positive with DOC ($r$ = 0.95, p = 0.003). dMeHg presented a significant positive correlation with pH ($r$ = 0.97, p = 0.028). pHg showed a significant negative correlation with salinity ($r$ = -0.94, p = 0.005), and significant positive correlations with DOC ($r$ = 0.88, p = 0.021) and dHg ($r$ = 0.89, p = 0.018; Fig. 3c).

## 4. Discussion

We measured a mean value of 16.6 ± 10.4 pM of tHg in Parnaiba waters, which is more similar to values reported for Hg in adjacent shelf than in tropical mangrove waters. For instance, in the Itacurussa Experimental Forest (IEF), located in moderately contaminated Sepetiba Bay in SE Brazil, and influenced by different rivers known to have anthropogenic loads of Hg, mean values for tHg in mangrove creek waters were 28.0 ± 2.5 pM, whereas for adjacent open bay waters, lowers values were obtained (19.0 ± 8.5 pM) (Lacerda et al., 2001b). The similarity in tHg concentrations between the mangrove and surrounding waters can be explained by the low anthropogenic inputs to the PRD and the influence of coastal waters on the system. The lower values of Hg (Hg: 0.15–4.90 ng $g^{-1}$) obtained in the Parnaiba sediments also corroborate the lack of a substantial anthropogenic input of Hg in the region. The riverside samples taken at P6 (Hg: 21.6–22.01 ng $g^{-1}$) and P7 (Hg: 26.7–28.2 ng $g^{-1}$) are typically fine-grained, organic matter-rich, reduced mangrove sediments, characteristics that result in a large capacity of trace metals accumulation (Lacerda et al., 2022). In agreement with our results, Hg concentrations in the bottom sediments of the Upper Parnaíba River were reported, ranging from 4.2 to 58.5 ng $g^{-1}$ (Remor et al., 2018). Similar concentrations of Hg in the bottom sediments were measured in other Brazilian mangrove-dominated estuarine areas of NE Brazil, the Jaguaribe River estuary, during the dry season (9.9 ng $g^{-1}$) (Moura and Lacerda, 2022), the Ceará river

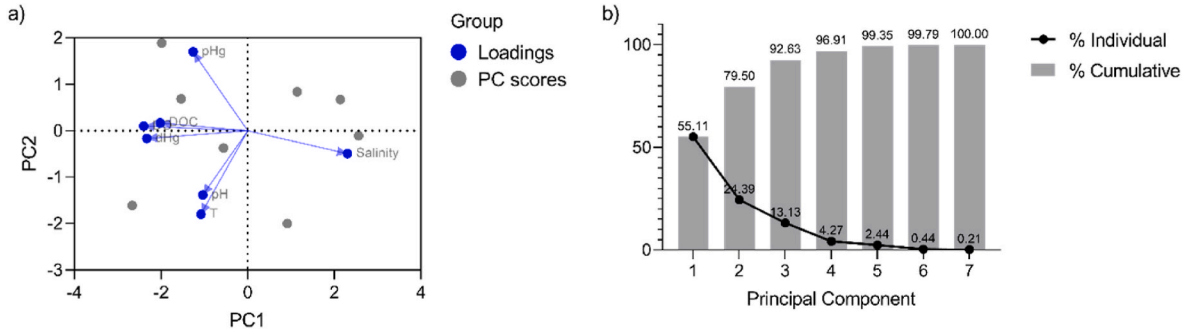


**Fig. 2.** a) Biplot for principal component analysis (PCA) of particulate mercury (pHg), dissolved mercury (dHg), and water column parameters (dissolved organic carbon – DOC, dissolved oxygen – DO, pH, temperature – T and salinity); b) Individual and cumulative variance accounted for by each principal component.

**Table 3**
Correlation matrix between total mercury (tHg) and dissolved methyl mercury (dMeHg) concentrations in water column, and in sediments (Hg sed) and water parameters at the studied hydrological stations (P1-12). Person's *r*, p value, and number of samples (n). Detailed statistical parameters are presented in Suppl. Mat. Table S1.

| | Salinity | T | DO | pH | DOC | pHg | dHg | dMeHg |
|---|---|---|---|---|---|---|---|---|
| T | r = −0.323 | | | | | | | |
| (n = 11) | p = 0.333 | | | | | | | |
| DO | r = −0.867 | r = 0.540 | | | | | | |
| (n = 11) | **p = 0.001** | p = 0.086 | | | | | | |
| pH | r = −0.048 | r = −0.020 | r = 0.015 | | | | | |
| (n = 11) | p = 0.889 | p = 0.952 | p = 0.966 | | | | | |
| DOC | r = −0.530 | r = 0.720 | r = 0.608 | r = −0.368 | | | | |
| (n = 11) | p = 0.093 | **p = 0.013** | **p = 0.047** | p = 0.266 | | | | |
| pHg | r = −0.357 | r = 0.216 | r = 0.415 | r = −0.257 | r = 0.644 | | | |
| (n = 11) | p = 0.281 | p = 0.523 | p = 0.205 | p = 0.445 | **p = 0.033** | | | |
| dHg | r = −0.793 | r = 0.367 | r = 0.849 | r = 0.494 | r = 0.711 | r = 0.385 | | |
| (n = 8) | **p = 0.019** | p = 0.371 | **p = 0.008** | p = 0.213 | **p = 0.048** | p = 0.347 | | |
| dMeHg | r = −0.842 | r = 0.326 | r = 0.835 | r = −0.005 | r = 0.491 | r = 0.580 | r = 0.640 | |
| (n = 9) | **p = 0.004** | p = 0.391 | **p = 0.005** | p = 0.989 | p = 0.180 | p = 0.102 | p = 0.122 | |
| Hg sed | r = 0.400 | r = 0.098 | r = −0.464 | r = −0.003 | r = −0.010 | r = −0.862 | r = 0.118 | r = −0.543 |
| (n = 7) | p = 0.374 | p = 0.834 | p = 0.294 | p = 0.994 | p = 0.984 | **p = 0.013** | p = 0.824 | p = 0.266 |

estuary (12.7 ng $g^{-1}$) (Morgado et al., 2021), and the Cayenne estuary in French Guiana (47–60 ng $g^{-1}$ of Hg) (Fiard et al., 2022; Michelet et al., 2021). These values are well below the legal limits defined by the national regulation CONAMA Resolution No. 454/2012 for coastal sediments (300–1000 ng $g^{-1}$). These results contrast with values reported on sediments of highly impacted subtropical mangrove areas, such as the industrialized Shenzhen Bay, South China, reaching 118 ng $g^{-1}$ Hg (Jiang et al., 2023), as well as, tropical mangrove areas with high industrial and urban pressure, such as the Salado estuary, Ecuador, that presented sediments with high concentrations of Hg (1200–2760 ng $g^{-1}$ dw) (Calle et al., 2018). tHg bioaccumulated in mussels inhabiting contaminated Salado estuary mangroves reached 4900 ± 760 ng $g^{-1}$ dw (Calle et al., 2018). As a comparison, PRD mangrove oysters show total Hg concentrations of 115 ± 31 ng $g^{-1}$ dw (V.L. Moura *pers. comm*). The fine-grained nature of mangrove sediments, combined with their high organic content, provides an ideal substrate for Hg adsorption (You et al., 2024). As pHg enters the system, it tends to be retained in organic-rich sediments. This process leads to a decrease in pHg in the water column, as observed in our study. The varying redox conditions in mangrove sediments, influenced by tidal cycles and organic matter decomposition, affect Hg speciation and partitioning. Under reducing conditions, Hg tends to form stable complexes with sulfides, further increasing its retention in sediments (Molina et al., 2023).

The dynamic behavior observed towards the end of the dry period, characterized by an already large supply of freshwater in the estuary system (Suppl. Mat. Fig. S2), has implications for the distribution and transport of Hg in the mangrove waters of the PRD. Specifically, the large supply of freshwater can affect the salinity of the mangrove waters (Chielle et al., 2023), which in turn can impact the solubility and mobility of Hg in the system (Clarke et al., 2023). Additionally, the influx of freshwater can introduce new sources of Hg into the system, such as runoff from agricultural or industrial activities at the upper reaches of the river basin. Therefore, understanding the dynamics of the estuary system during the dry period is crucial for predicting and managing the distribution and transport of Hg in the PRD mangrove waters. Our findings highlight that salinity plays a crucial role in shaping Hg distribution patterns along the estuarine gradient. We measured lower values of tHg (4.27–23.51 pM) at stations P4, P5, P9, P10 and P12. These stations are located at the mouth of the Parnaíba River estuary, the Cajú Bay, and the Manceieira Bay, which are areas with higher volumes of seawater mixing (Suppl. Mat. Fig. S2). Typical Atlantic Ocean seawater Hg levels 0.80 ± 0.42 pM (Cossa et al., 2018; Torres-Rodriguez et al., 2024). The negative correlations observed between salinity and the quantified Hg fractions are in agreement with commonly reported progressive decreases in the dHg with seawater mixing at the lower estuary areas (Lei et al., 2019), but also in other wetlands formed in the intertidal zone of sheltered coasts, such as a salt marsh in Massachusetts, USA (Wang and Obrist, 2022). Studies have shown that salinity gradients can impact the transformation and complexation of Hg species (Eom et al., 2024), affecting their potential toxicity and bioaccumulation in aquatic organisms (Moura and Lacerda, 2022). Therefore, the observed salinity profiles should be considered when assessing the distribution and fate of Hg in the PRD. The longitudinal changes in salinity and pH gradients due to the mix of freshwater and seawater along the PRD have also been observed to lead to a variability of the physicochemical conditions, playing a key role in the partitioning of trace metals, with a reduction of trace metals concentration with increased salinity and pH (Santos et al., 2024).

In our study, the contribution of pH to the partitioning of Hg in mangrove waters is more obvious during the 24 h tidal cycle evaluation. In general, we observed lower dHg values at points with higher pH, and higher dMeHg with increased pH. The influence of pH on Hg species and bioaccumulation in estuarine environments is a multifaceted issue involving chemical speciation, organic matter interactions, and biological processes (Ullrich et al., 2001b). Lower pH generally increases Hg solubility and availability due to strong proton competition for the Hg (II) binding sites (Haitzer et al., 2003). On the other hand, pH also contributes to changes on DOM conformation, which might alter how effectively DOC binds to Hg. Thus, changes in water chemistry, such as pH, redox potential, ionic strength, DOM, affect the size and structure of colloids, influencing the affinity for Hg (Aiken et al., 2011). Higher DOC concentrations in low-salinity sampling sites positively correlate with higher dHg, suggesting a possible exchange between the particulate and dissolved Hg phases as previously reported in mangrove-based estuaries (Bergamaschi et al., 2012; Marins et al., 1997; Martins et al., 2002; Mounier et al., 2001). The dominant role of Hg complexes with DOC has been previously highlighted for the tropical mangrove water from IEF, Brazil (Lacerda et al., 2001a). Incubation studies with mangrove sediments from SE Brazil (Correia and Guimarães, 2017; De Oliveira et al., 2015) found higher Hg methylation in the superficial fraction of sediments varying from 0.5 to 7.8 % of the tHg concentration. In addition, plant roots and litter can also contribute to MeHg formation. MeHg formation in sediment also tended to increase with salinity, suggesting that sulfate-reducing bacteria (SRB) are important Hg methylators in mangrove sediments, acting in conjunction with iron-reducing (IRB) and methanogens. Cossa et al. (2014) developed a Michaelis-Menten type equation to describe the complex relationship between inorganic mercury (iHg) in sediments and MeHg production. Their model shows that MeHg production increases linearly with iHg at low concentrations, but this rate slows and eventually plateaus as iHg levels rise. This suggests a

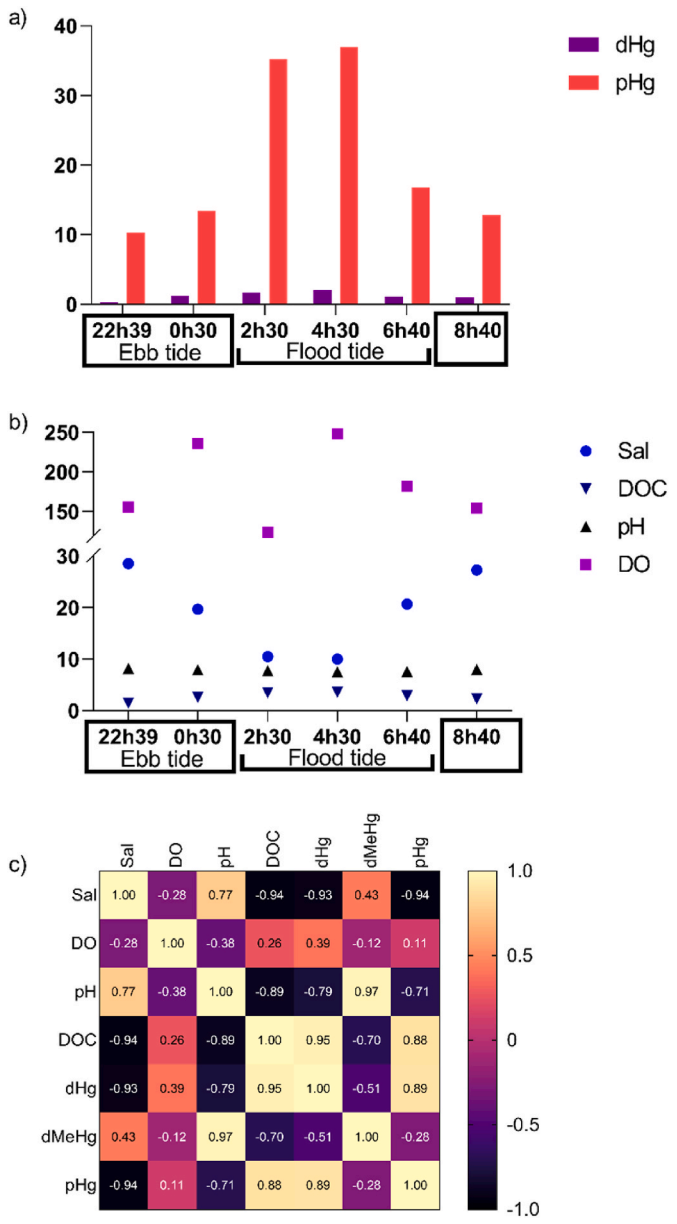


**Fig. 3.** Graphical representation of the data obtained at the hydrological station P8 during a tidal cycle; a) particulate (pHg) and dissolved (dHg) mercury concentration (pM); b) tidal variability of water parameters; c) heatmap for Pearson's r value for the correlation between water parameters and the dissolved and particulate Hg fractions.

saturation point exists, beyond which additional iHg does not significantly increase MeHg production due to limiting factors such as electron donor availability, microbial activity, and other environmental conditions. The presence of labile terrestrial DOC and a shift in ionic strength and microbial activity during the transition into saline waters within estuaries were therefore suggested as facilitators of the methylation process. Accordingly, we observed increased dHg and dMeHg with increased DO values along the sampling sites. Schartup et al. (2015) employed enriched Hg isotope incubation, revealing active Hg methylation in oxic estuarine seawater on the Northwest Atlantic continental margin. Microbial consortia, including, for example, SRB and methanogenic archaea, are believed to play a central role in driving the methylation process, as evidenced in Coroa Grande mangrove sediments (Sepetiba Bay, Rio de Janeiro, Brazil) (Correia and Guimarães, 2017). The efficiency of this process is contingent not only on microbial composition and activity but also on the presence of both organic and inorganic complexing agents in the medium (Ullrich et al., 2001b). Redox gradients are known to drive Hg speciation with the highest MeHg concentrations typically observed in anoxic waters (Cabrol et al., 2023; Rosati et al., 2018). Despite the global trend of decreasing DO levels in coastal and marine environments (Calle et al., 2018), the present study revealed high concentrations of DO throughout the water column, because of the high circulation and saline water penetration throughout the estuary (Chielle et al., 2023), and exceeding the minimum threshold of 5.7 mg $L^{-1}$ (178 μM) established by regulatory agencies such as Brazilian regulation (CONAMA no. 357, March 17, 2005).

The interaction between water physicochemical parameters and Hg speciation in the PRD waters is well illustrated by the 24 h sampling at P8, a station located in the estuarine mixing zone, representing the typical mixture between fresh and marine water, but with a contribution from the surrounding mangroves and their export of surface and porewaters during ebb periods. In contrast with the decrease in dHg levels with salinity increase, higher dHg concentrations have been observed under higher DOC levels, as observed by previous studies on mangroves in Florida, USA (Bergamaschi et al., 2012). Higher values of dHg were observed during the flood tide period. This may be related to an enrichment of the flood water on Hg as they traverse mud flats where pore waters harbor higher Hg concentrations, reaching up to 14.3 pM. Lacerda et al. (2001b) suggested mud flats pore water as the major source of Hg along with facilitation of Hg migration associated with increased DOC. This association has been reported to transport Hg from mangrove creek waters and mudflat porewaters in subtropical (Mounier et al., 2001) and tropical semi-arid (Martins et al., 2002) estuaries. Mercury complexation with DOC can increase the mobility and bioavailability of Hg in adjacent coastal waters (Moura and Lacerda, 2022). We observed that dMeHg accounted for 2 - 12 % of the total dHg during the tidal cycle, which is within the range reported in subtropical and tropical estuaries (0.5 - 40%) (Lei et al., 2019). The bioavailable dMeHg, the Hg species of major concern regarding ecosystem and human health, presented a strong positive correlation with pH and a negative one with DOC. In agreement with our results, the presence of organic matter in mangrove sediments has been described as an important regulating agent of the dynamics of Hg methylation, as organic matter can bind to Hg, affecting its bioavailability for methylation (Liu et al., 2022).

The observed greater riverine contribution during ebb tide conditions indicates freshwater input's importance in the region, even during the dry period. The transport and remobilization of legacy Hg from upstream sources, such as industrial and agricultural activities, can be facilitated during periods of higher river discharge events, potentially influencing the distribution and accumulation of Hg in the estuarine environment (Moura and Lacerda, 2022). However, during drought periods, longer water retention in estuaries can affect sediment transport, leading to changes in Hg concentrations in water and sediments (Lacerda et al., 2020; Moura and Lacerda, 2022). The increased residence time of water in estuaries can also lead to greater mobilization of bioavailable Hg, which can accelerate Hg bioaccumulation in aquatic ecosystems (Morgado et al., 2021). Consequently, the increasing mobilization and bioavailability of Hg within estuarine ecosystems emerge as a pervasive and environmentally consequential outcome attributed to worsened drought conditions due to excessive water resource utilization, reduced annual precipitation, and the occurrence of more prolonged drought events induced by global climate change (Lacerda et al., 2020).

## 5. Conclusions

In summary, the hydrodynamic features of the Parnaíba River Delta, encompassing factors such as freshwater input, salinity gradients, pH variations, dissolved oxygen levels, and flow patterns, exert a

noteworthy influence on the distribution and behavior of Hg in mangrove dominated estuaries. Our findings indicate that the mangrove ecosystem in the Parnaíba region maintains a pristine state with low Hg concentrations in both water and sediment. This includes a low abundance of dMeHg, suggesting a limited risk/potential of bioaccumulation in the PRD and similar mangrove systems. These characteristics emphasize the critical role of mangroves as natural biogeochemical buffers, which effectively trap and retain Hg within their sediment and high organic carbon content, thereby potentially reducing Hg mobility. These findings support the ecological importance of mangrove systems in mitigating Hg contamination, reinforcing their value in protecting coastal biodiversity and reducing Hg export to the ocean. These investigations are vital for devising effective management strategies to mitigate the risks associated with Hg contamination in such an ecologically unique habitat such as the PRD, as well as analogous estuarine systems between the Amazon and the Brazilian semi-arid region, especially under a changing climate. Pristine mangrove systems are effectively sequestering carbon and mercury and can, therefore, be considered as blue carbon and blue mercury ecosystems.

## CRediT authorship contribution statement

**Andreia C.M. Rodrigues:** Writing – original draft, Formal analysis. **Natalia Torres-Rodriguez:** Writing – review & editing, Investigation. **Jingjing Yuan:** Writing – review & editing, Investigation. **Aurélie Dufour:** Resources. **Luiz Drude de Lacerda:** Writing – review & editing, Investigation, Funding acquisition, Conceptualization. **Lars-Eric Heimbürger-Boavida:** Writing – review & editing, Methodology, Investigation, Funding acquisition, Formal analysis, Conceptualization.

## Declaration of competing interest

The authors declare that they have no known competing financial interests or personal relationships that could have appeared to influence the work reported in this paper.

## Acknowledgments

The authors would like to thank members of the Coastal Biogeochemistry for helping with the sampling and analysis. To Rozane Valente Marins as coordinator of PRONEX (PR2-0101-00052.01.00/15), which financed the Delta missions. This research was funded by Brazilian-French cooperation agreement (CAPES-CPECUB (UFC/U. Toulon-MIO) Project No. 88881.370863/2019-1. This study is also an output of the INCT Continent-Ocean Materials Transfer (INCT-TMC Ocean supported by Conselho Nacional de Desenvolvimento Científico e Tecnológico - CNPq Proc. No. 405.765/2022–3 to LD Lacerda. Andreia C. M. Rodrigues would like to thanks the European Union's Horizon 2020 research and innovation programme under grant agreement N°101034324 and the French government under the France 2030 investment plan, as part of the Initiative d'Excellence d'Aix-Marseille Université – A*MIDEX AMX- 22-CIVIS3i-PF-0045. We would like to thank Tristan Rousseau, Maria Montero Curiel and Stéphane Mounier for their support.

## Appendix A. Supplementary data

Supplementary data to this article can be found online at https://doi.org/10.1016/j.chemosphere.2025.144262.

## Data availability

Data will be made available on request.

## References

Aiken, G.R., Hsu-Kim, H., Ryan, J.N., 2011. Influence of dissolved organic matter on the environmental fate of metals, nanoparticles, and colloids. Environ. Sci. Technol. 45, 3196–3201. https://doi.org/10.1021/es103992s.

Aleku, D.L., Lazareva, O., Pichler, T., 2024. Mercury in groundwater – source, transport and remediation. Appl. Geochem. 170, 106060. https://doi.org/10.1016/j.apgeochem.2024.106060.

Andrade, A.S.J., Bastos, E.A., Barros, H.C., Silva, C.O., Gomes, A.A.N., 2005. Classificação climática e regionalização do semi-árido do estado do Piauí. Rev. Cienc. Agron. 36, 143–151.

Awuku-Sowah, E.M., Graham, N.A.J., Watson, N.M., 2022. Investigating mangrove-human health relationships: a review of recently reported physiological benefits. Dialogues in Health 1, 100059. https://doi.org/10.1016/j.dialog.2022.100059.

Bergamaschi, B.A., Krabbenhoft, D.P., Aiken, G.R., Patino, E., Rumbold, D.G., Orem, W. H., 2012. Tidally driven export of dissolved organic carbon, total mercury, and methylmercury from a mangrove-dominated estuary. Environ. Sci. Technol. 46, 1371–1378. https://doi.org/10.1021/es2029137.

Bittencourt, A.C.D.S.P., Dominguez, J.M.L., Martin, L., Silva, I.R., 2005. Longshore transport on the northeastern Brazilian coast and implications to the location of large scale accumulative and erosive zones: an overview. Mar. Geol. 219, 219–234. https://doi.org/10.1016/j.margeo.2005.06.006.

Cabral, A., Yau, Y.Y.Y., Reithmaier, G.M.S., Cotovicz, L.C., Barreira, J., Broström, G., Viana, B., Fonseca, A.L., Santos, I.R., 2024. Tidally driven porewater exchange and diel cycles control CO2 fluxes in mangroves on local and global scales. Geochem. Cosmochim. Acta 374, 121–135. https://doi.org/10.1016/j.gca.2024.04.020.

Cabrol, L., Capo, E., Van Vliet, D.M., Von Meijenfeldt, F.A.B., Bertilsson, S., Villanueva, L., Sánchez-Andrea, I., Björn, E., G Bravo, A., Heimburger Boavida, L.-E., 2023. Redox gradient shapes the abundance and diversity of mercury-methylating microorganisms along the water column of the Black Sea. mSystems e00537–23. https://doi.org/10.1128/msystems.00537-23.

Calle, P., Monserrate, L., Medina, F., Calle Delgado, M., Tirapé, A., Montiel, M., Ruiz Barzola, O., Cadena, O.A., Dominguez, G.A., Alava, J.J., 2018. Mercury assessment, macrobenthos diversity and environmental quality conditions in the Salado Estuary (Gulf of Guayaquil, Ecuador) impacted by anthropogenic influences. Mar. Pollut. Bull. 136, 365–373. https://doi.org/10.1016/j.marpolbul.2018.09.018.

Castro, S., Luiz-Silva, W., Machado, W., Valezio, E., 2021. Mangrove sediments as long-term mercury sinks: evidence from millennial to decadal time scales. Mar. Pollut. Bull. 173, 113031. https://doi.org/10.1016/j.marpolbul.2021.113031.

Chielle, R.S.A., Marins, R.V., Cavalcante, M.S., Cotovicz, L.C., 2023. Seasonal and spatial variability of $CO_2$ emissions in a large tropical mangrove-dominated delta. Limnology & Oceanography lno 12471. https://doi.org/10.1002/lno.12471.

Clarke, R.G., Klapstein, S.J., Keenan, R., O'Driscoll, N.J., 2023. Mercury photoreduction and photooxidation kinetics in estuarine water: effects of salinity and dissolved organic matter. Chemosphere 312, 137279. https://doi.org/10.1016/j.chemosphere.2022.137279.

Coquery, M., Cossa, D., Martin, J.M., 1995. The distribution of dissolved and particulate mercury in three Siberian estuaries and adjacent Arctic coastal waters. Water Air Soil Pollut. 80, 653–664. https://doi.org/10.1007/BF01189718.

Correia, R.R.S., Guimarães, J.R.D., 2017. Mercury methylation and sulfate reduction rates in mangrove sediments, Rio de Janeiro, Brazil: the role of different microorganism consortia. Chemosphere 167, 438–443. https://doi.org/10.1016/j.chemosphere.2016.09.153.

Cossa, D., Dang, D.H., Thomas, B., 2024. Mercury mobility in epibenthic waters of a deltaic environment. JGR Biogeosciences 129, e2023JG007575. https://doi.org/10.1029/2023JG007575.

Cossa, D., Durrieu De Madron, X., Schäfer, J., Guédron, S., Marusczak, N., Castelle, S., Naudin, J.-J., 2018. Sources and exchanges of mercury in the waters of the Northwestern Mediterranean margin. Prog. Oceanogr. 163, 172–183. https://doi.org/10.1016/j.pocean.2017.05.002.

Cossa, D., Garnier, C., Buscail, R., Elbaz-Poulichet, F., Mikac, N., Patel-Sorrentino, N., Tessier, E., Rigaud, S., Lenoble, V., Gobeil, C., 2014. A Michaelis–Menten type equation for describing methylmercury dependence on inorganic mercury in aquatic sediments. Biogeochemistry 119, 35–43. https://doi.org/10.1007/s10533-013-9924-3.

De Oliveira, D.C.M., Correia, R.R.S., Marinho, C.C., Guimarães, J.R.D., 2015. Mercury methylation in sediments of a Brazilian mangrove under different vegetation covers and salinities. Chemosphere 127, 214–221. https://doi.org/10.1016/j.chemosphere.2015.02.009.

Diniz, C., Cortinhas, L., Nerino, G., Rodrigues, J., Sadeck, L., Adami, M., Souza-Filho, P., 2019. Brazilian mangrove status: three decades of satellite data analysis. Remote Sens. 11, 808. https://doi.org/10.3390/rs11070808.

Eom, S., Kim, J., Jung, E., Kwon, S.Y., Hong, Y., Lee, M., Park, J.H., Han, S., 2024. Effects of hydrologic regimes on the loading and spatiotemporal variation of mercury in the microtidal river estuary. Mar. Pollut. Bull. 205, 116602. https://doi.org/10.1016/j.marpolbul.2024.116602.

Fiard, M., Cuny, P., Sylvi, L., Hubas, C., Jézéquel, R., Lamy, D., Walcker, R., El Houssainy, A., Heimbürger-Boavida, L.-E., Robinet, T., Bihannic, I., Gilbert, F., Michaud, E., Dirberg, G., Militon, C., 2022. Mangrove microbiota along the urban-to-rural gradient of the Cayenne estuary (French Guiana, South America): drivers and potential bioindicators. Sci. Total Environ. 807, 150667. https://doi.org/10.1016/j.scitotenv.2021.150667.

Fisher, J.A., Jacob, D.J., Soerensen, A.L., Amos, H.M., Steffen, A., Sunderland, E.M., 2012. Riverine source of Arctic Ocean mercury inferred from atmospheric observations. Nat. Geosci. 5, 499–504. https://doi.org/10.1038/ngeo1478.

Fitzgerald, W.F., Lamborg, C.H., Hammerschmidt, C.R., 2007. Marine biogeochemical cycling of mercury. Chem. Rev. 107, 641–662. https://doi.org/10.1021/cr050353m.
GEOTRACES, 2017. Cookbook version 3, p 66-76. Sampling and Sample-handling Protocols.
Gworek, B., Bemowska-Kałabun, O., Kijeńska, M., Wrzosek-Jakubowska, J., 2016. Mercury in marine and oceanic waters—a review. Water Air Soil Pollut. 227, 371. https://doi.org/10.1007/s11270-016-3060-3.
Haitzer, M., Aiken, G.R., Ryan, J.N., 2003. Binding of mercury(II) to aquatic humic substances: influence of pH and source of humic substances. Environ. Sci. Technol. 37, 2436–2441. https://doi.org/10.1021/es026291o.
Hastenrath, S., 2006. Circulation and teleconnection mechanisms of Northeast Brazil droughts. Prog. Oceanogr. 70, 407–415. https://doi.org/10.1016/j.pocean.2005.07.004.
Heimbürger, L.-E., Sonke, J.E., Cossa, D., Point, D., Lagane, C., Laffont, L., Galfond, B.T., Nicolaus, M., Rabe, B., van der Loeff, M.R., 2015. Shallow methylmercury production in the marginal sea ice zone of the central Arctic Ocean. Sci. Rep. 5, 10318. https://doi.org/10.1038/srep10318.
Horvat, M., 1997. Mercury behaviour in estuarine and coastal, transactions on ecology and the environment. Transactions on Ecology and the Environment 14.
Huang, S., Jiang, R., Song, Q., Zhang, Y., Huang, Q., Su, B., Chen, Y., Huo, Y., Lin, H., 2020. Study of mercury transport and transformation in mangrove forests using stable mercury isotopes. Sci. Total Environ. 704, 135928. https://doi.org/10.1016/j.scitotenv.2019.135928.
Jiang, J.J., Yan, H., Wang, X., Su, H., 2023. Sediment mercury concentration of a subtropical mangrove wetland responded to Hong Kong-Shenzhen industrial development since the 1960s. Mar. Pollut. Bull. 192, 115047. https://doi.org/10.1016/j.marpolbul.2023.115047.
Jiskra, M., Heimbürger-Boavida, L.-E., Desgranges, M.-M., Petrova, M.V., Dufour, A., Ferreira-Araujo, B., Masbou, J., Chmeleff, J., Thyssen, M., Point, D., Sonke, J.E., 2021. Mercury stable isotopes constrain atmospheric sources to the ocean. Nature 597, 678–682. https://doi.org/10.1038/s41586-021-03859-8.
Lacerda, L.D., Marins, R.V., Dias, F.J.D.S., 2020. An arctic paradox: response of fluvial Hg inputs and bioavailability to global climate change in an extreme coastal environment. Front. Earth Sci. 8, 93. https://doi.org/10.3389/feart.2020.00093.
Lacerda, L.D., Marins, R.V., Paraquetti, H.H.M., Mounier, S., Benaim, J., Fevrier, D., 2001a. Mercury distribution and reactivity in waters of a subtropical coastal lagoon, Sepetiba Bay, SE Brazil. J. Braz. Chem. Soc. 12. https://doi.org/10.1590/S0103-50532001000100013.
Lacerda, L.D., Silva, L.F.F., Marins, R.V., Mounier, S., Paraquetti, H.H.M., Benaim, J., 2001b. Dissolved mercury concentrations and reactivity in mangrove waters from the Itacurussa experimental forest, Sepetiba bay, SE Brazil. Wetl. Ecol. Manag. 9, 323–331. https://doi.org/10.1023/A:1011868803439.
Lacerda, L.D., Ward, R.D., Borges, R., Ferreira, A.C., 2022. Mangrove trace metal biogeochemistry response to global climate change. Front. For. Glob. Change 5, 817992. https://doi.org/10.3389/ffgc.2022.817992.
Lamborg, C.H., Hammerschmidt, C.R., Bowman, K.L., 2016. An examination of the role of particles in oceanic mercury cycling. Phil. Trans. R. Soc. A. 374, 20150297. https://doi.org/10.1098/rsta.2015.0297.
Lei, P., Zhong, H., Duan, D., Pan, K., 2019. A review on mercury biogeochemistry in mangrove sediments: hotspots of methylmercury production? Sci. Total Environ. 680, 140–150. https://doi.org/10.1016/j.scitotenv.2019.04.451.
Liem-Nguyen, V., Jonsson, S., Skyllberg, U., Nilsson, M.B., Andersson, A., Lundberg, E., Björn, E., 2016. Effects of nutrient loading and mercury chemical speciation on the formation and degradation of methylmercury in estuarine sediment. Environ. Sci. Technol. 50, 6983–6990. https://doi.org/10.1021/acs.est.6b01567.
Liu, J., Li, Y., Duan, D., Peng, G., Li, P., Lei, P., Zhong, H., Tsui, M.T.-K., Pan, K., 2022. Effects and mechanisms of organic matter regulating the methylmercury dynamics in mangrove sediments. J. Hazard Mater. 432, 128690. https://doi.org/10.1016/j.jhazmat.2022.128690.
Liu, M., Zhang, Q., Maavara, T., Liu, S., Wang, X., Raymond, P.A., 2021. Rivers as the largest source of mercury to coastal oceans worldwide. Nat. Geosci. 14, 672–677. https://doi.org/10.1038/s41561-021-00793-2.
Marins, R.V., Lacerda, L.D., Gonçalves, G.O., Paiva, E.C., 1997. Effect of root metabolism on the post-depositional mobilization of mercury in salt marsh soils. Bull. Environ. Contam. Toxicol. 58, 733–738.
Martins, R.V., Lacerda, L.D., Mounier, S., Paraquetti, H.H.M., Marques, W.S., 2002. Caracterização hidroquímica, distribuição e especiação de mercúrio nos estuários dos Rios Ceará e Pacotí, Região Metropolitana de Fortaleza, Ceará, Brasil. Geochim. Bras. 16, 37.
Menéndez, P., Losada, I.J., Torres-Ortega, S., Narayan, S., Beck, M.W., 2020. The global flood protection benefits of mangroves. Sci. Rep. 10, 4404. https://doi.org/10.1038/s41598-020-61136-6.
Michelet, C., Zeppilli, D., Hubas, C., Baldrighi, E., Cuny, P., Dirberg, G., Militon, C., Walcker, R., Lamy, D., Jézéquel, R., Receveur, J., Gilbert, F., Houssainy, A.E., Dufour, A., Heimbürger-Boavida, L.-E., Bihannic, I., Sylvi, L., Vivier, B., Michaud, E., 2021. First assessment of the benthic meiofauna sensitivity to low human-impacted mangroves in French Guiana. Forests 12, 338. https://doi.org/10.3390/f12030338.
Molina, A., Duque, G., Cogua, P., 2023. Effect of environmental variables on mercury accumulation in sediments of an anthropogenically impacted tropical estuary (Buenaventura Bay, Colombian Pacific). Environ. Monit. Assess. 195, 1316. https://doi.org/10.1007/s10661-023-11721-9.
Monperrus, M., Tessier, E., Veschambre, S., Amouroux, D., Donard, O., 2005. Simultaneous speciation of mercury and butyltin compounds in natural waters and snow by propylation and species-specific isotope dilution mass spectrometry analysis. Anal. Bioanal. Chem. 381, 854–862. https://doi.org/10.1007/s00216-004-2973-7.
Morgado, F., Santos, R.M.A.L., Sampaio, D., De Lacerda, L.D., Soares, A.M.V.M., Vieira, H.C., Abreu, S., 2021. Chronological trends and mercury bioaccumulation in an aquatic semiarid ecosystem under a global climate change scenario in the northeastern coast of Brazil. Animals 11, 2402. https://doi.org/10.3390/ani11082402.
Mounier, S., Lacerda, L.D., Marins, R.V., Bemaim, J., 2001. Copper and mercury complexing capacity of organic matter from a mangrove mud flat environment, Sepetiba bay, Brazil. Bull. Environ. Contam. Toxicol. 67, 519–525. https://doi.org/10.1007/s001280154.
Moura, V.L., Lacerda, L.D., 2022. Mercury sources, emissions, distribution and bioavailability along an estuarine gradient under semiarid conditions in northeast Brazil. IJERPH 19, 17092. https://doi.org/10.3390/ijerph192417092.
Outridge, P.M., Mason, R.P., Wang, F., Guerrero, S., Heimbürger-Boavida, L.E., 2018. Updated global and oceanic mercury budgets for the united nations global mercury assessment 2018. Environ. Sci. Technol. acs.est.8b01246. https://doi.org/10.1021/acs.est.8b01246.
Paula Filho, F.J., Marins, R.V., De Lacerda, L.D., 2015. Natural and anthropogenic emissions of N and P to the Parnaíba River delta in NE Brazil. Estuarine. Coastal and Shelf Science 166, 34–44. https://doi.org/10.1016/j.ecss.2015.03.020.
Paula Filho, F.J., Marins, R.V., Santos, D.V., Pereira Junio, R.F., Menezes, J.M.C., Da Gastão, F.G.C., Guzzi, A., Teixeira, R.N.P., 2021. Assessment of heavy metals in sediments of the Parnaíba River Delta in the semi-arid coast of Brazil. Environ. Earth Sci. 80, 167. https://doi.org/10.1007/s12665-021-09456-2.
Remor, M.B., Sampaio, S.C., Rosa, D.M., Model, K.J., Paloschi, C.L., Conceição, F.G.D., 2018. Mercury in the sediment of the upper parnaíba river. Eng. Agríc. 38, 760–767. https://doi.org/10.1590/1809-4430-eng.agric.v38n5p760-767/2018.
Rosati, G., Heimbürger, L.E., Melaku Canu, D., Lagane, C., Laffont, L., Rijkenberg, M.J.A., Gerringa, L.J.A., Solidoro, C., Gencarelli, C.N., Hedgecock, I.M., De Baar, H.J.W., Sonke, J.E., 2018. Mercury in the black sea: new insights from measurements and numerical modeling. Glob. Biogeochem. Cycles 32, 529–550. https://doi.org/10.1002/2017GB005700.
Rovai, A.S., Twilley, R.R., Worthington, T.A., Riul, P., 2022. Brazilian mangroves: blue carbon hotspots of national and global relevance to natural climate solutions. Front. For. Glob. Change 4, 787533. https://doi.org/10.3389/ffgc.2021.787533.
Santos, T.T.L., Mounier, J.L.S., Marins, R.V., 2024. Trace metal partitioning in the Parnaíba delta in dry season, equatorial coast of Brazil. Environ. Pollut. 345, 123500. https://doi.org/10.1016/j.envpol.2024.123500.
Santos, V.H.M., Lima, H.P., 2022. Delta do Rio Parnaíba. Vazão e parâmetro físico-químicos. UFMA, São Luís 17.
Schartup, A.T., Ndu, U., Balcom, P.H., Mason, R.P., Sunderland, E.M., 2015. Contrasting effects of marine and terrestrially derived dissolved organic matter on mercury speciation and bioavailability in seawater. Environ. Sci. Technol. 49, 5965–5972. https://doi.org/10.1021/es506274x.
SNIRH, 2023. Hydroweb: Rede Hidrometeorológica Nacional. Agência Nacional de Águas (ANA), Brasília, DF.
Soares, M.O., Campos, C.C., Carneiro, P.B.M., Barroso, H.S., Marins, R.V., Teixeira, C.E.P., Menezes, M.O.B., Pinheiro, L.S., Viana, M.B., Feitosa, C.V., Sánchez-Botero, J.I., Bezerra, L.E.A., Rocha-Barreira, C.A., Matthews-Cascon, H., Matos, F.O., Gorayeb, A., Cavalcante, M.S., Moro, M.F., Rossi, S., Belmonte, G., Melo, V.M.M., Rosado, A.S., Ramires, G., Tavares, T.C.L., Garcia, T.M., 2021. Challenges and perspectives for the Brazilian semi-arid coast under global environmental changes. Perspectives in Ecology and Conservation 19, 267–278. https://doi.org/10.1016/j.pecon.2021.06.001.
Sonke, J.E., Heimbürger, L.-E., Dommergue, A., 2013. Mercury biogeochemistry: paradigm shifts, outstanding issues and research needs. C. R. Geosci. 345, 213–224. https://doi.org/10.1016/j.crte.2013.05.002.
Szczygielski, A., Stattegger, K., Schwarzer, K., Da Silva, A.G.A., Vital, H., Koenig, J., 2015. Evolution of the Parnaíba delta (NE Brazil) during the late holocene. Geo Mar. Lett. 35, 105–117. https://doi.org/10.1007/s00367-014-0395-x.
Tesán-Onrubia, J.A., Petrova, M.V., Puigcorbé, V., Black, E.E., Valk, O., Dufour, A., Hamelin, B., Buesseler, K.O., Masqué, P., Le Moigne, F.A.C., Sonke, J.E., Rutgers Van Der Loeff, M., Heimbürger-Boavida, L.-E., 2020. Mercury export flux in the arctic ocean estimated from $^{234}$Th/$^{238}$U disequilibria. ACS Earth Space Chem. 4, 795–801. https://doi.org/10.1021/acsearthspacechem.0c00055.
Torres-Rodriguez, N., Yuan, J., Petersen, S., Dufour, A., González-Santana, D., Chavagnac, V., Planquette, H., Horvat, M., Amouroux, D., Cathalot, C., Pelleter, E., Sun, R., Sonke, J.E., Luther, G.W., Heimbürger-Boavida, L.-E., 2024. Mercury fluxes from hydrothermal venting at mid-ocean ridges constrained by measurements. Nat. Geosci. 17, 51–57. https://doi.org/10.1038/s41561-023-01341-w.
Ullrich, S.M., Tanton, T.W., Abdrashitova, S.A., 2001a. Mercury in the aquatic environment: a review of factors affecting methylation. Crit. Rev. Environ. Sci. Technol. 31, 241–293. https://doi.org/10.1080/20016491089226.
Ullrich, S.M., Tanton, T.W., Abdrashitova, S.A., 2001b. Mercury in the aquatic environment: a review of factors affecting methylation. Crit. Rev. Environ. Sci. Technol. 31, 241–293. https://doi.org/10.1080/20016491089226.
Velásquez-López, P.C., López-Sánchez, I.Y., Rivera-Velásquez, M.F., 2020. Estimation of the ecological and human health risk of mercury in a mangrove area of the La Puntilla estuary, El Oro province, southern Ecuador. Bol. Invest. Mar. Costeras 49, 81–100. https://doi.org/10.25268/bimc.invemar.2020.49.1.775.
Viana, A.P., Le Loc'h, F., Frédou, T., Lucena-Frédou, F., Ménard, F., Lagane, C., Munaron, J.-M., Lira, A.S., Dos Santos, Í.G.S., Ferreira, V., Gonzalez, J.G., Point, D., 2023. Mercury biomagnification and trophic structure patterns in neotropical coastal estuaries impacted by a Chlor-alkali plant in northeast Brazil. Regional Studies in Marine Science 66, 103105. https://doi.org/10.1016/j.rsma.2023.103105.

Villar, E., Cabrol, L., Heimbürger-Boavida, L., 2020. Widespread microbial mercury methylation genes in the global ocean. Environ Microbiol Rep 12, 277–287. https://doi.org/10.1111/1758-2229.12829.

Wang, T., Obrist, D., 2022. Inorganic and methylated mercury dynamics in estuarine water of a salt marsh in Massachusetts, USA. Environ. Pollut. 294, 118657. https://doi.org/10.1016/j.envpol.2021.118657.

You, X., Sun, L., Chen, X., Li, Y., Zheng, J., Yuan, D., Wu, J., Sun, S., 2024. Mercury distribution and transfer in mangrove forests in urban areas under simulated rising sea levels. Front. Mar. Sci. 11. https://doi.org/10.3389/fmars.2024.1444302.

INMET, 2023. Instituto Nacional de Meteorologia. Ministério da Agricultura e Pecuária, December Brasília, DF. http://www.inmet.gov.br/portal/index.php?r=bdmep/bdmep. Assessed in December 2023.